Electronic Supplementary Information

Mesoporous silicas tethered with anions as quasi-solid electrolyte for lithium-metal batteries

Zerui Chen[a], Yifei Xu[a], Wei Zhao[a], Qianqian Liu[a,b], Qian Liu[a], Zhikun Hu[a], Yan Liu[a], Hao Bin Wu[a,*]

[a]Institute for Composites Science Innovation (InCSI) and State Key Laboratory of Silicon Materials, School of Materials Science and Engineering, Zhejiang University, Hangzhou 310027, P. R. China

[b]Key Laboratory of Electronic Materials and Devices of Tianjin, School of Electronics and Information Engineering, Hebei University of Technology, Tianjin, China

Email: hbwu@zju.edu.cn (H. B. Wu)

Methods

Materials

All chemical reagents such as (3-mercaptopropyl)trimethoxysilane (MPTMS) , (3-Aminopropyl)triethoxysilane (APTES), trifluoromethanesulfonic anhydride (Tf_2O), N-methyl pyrrolidone (NMP), anhydrous dichloromethane (CH_2Cl_2), were purchased from Aladdin Industrial Corporation. Toluene, ethanol, sulfuric acid, triethylamine (Et_3N), pyridine(Py) were purchased from China National Medicines Corporation Ltd. Lithium bis(trifluoromethanesulfonyl)imide (LiTFSI) were purchased from Guotai super power. All of the chemicals were used directly without further purification.

Synthesis of -SO_3H-functionalized mesoporous silicas (MCM41-SO_3H, SBA15-SO_3H)

-SO_3H-functionalized mesoporous silicas were synthesis by the two-step method[1]. -SH-functionalized mesoporous silicas were firstly prepared by treating the mesoporous silicas (MCM41, SBA15) with MPTMS. Briefly, 1.0 g mesoporous silicas were added to a solution of MPTMS (2 mL) in dry toluene and refluxed for 24 h. The products were collected by centrifugation, washed with toluene and ethanol for several times and dried at 110 ℃ for 5 h (denoted as MCM41-SH, SBA15-

SH).

The formation of -SO_3H group was realized by oxidation of -SH group. The mixture of SH-functionalized mesoporous silicas (1.0 g) (MCM41-SH, SBA15-SH), 30% H_2O_2 solution (10 mL) and concentrate H_2SO_4 (0.0156 g, 0.16 mmol) was stirred at room temperature for 20 h. The solid was collected by centrifugation and washed with deionized water until the washings were neutral. In order to confirm that all the -SO_3H groups were protonated, the solid was further suspended in 0.05 M H_2SO_4 (6 mL) for 5 h. The solid was then washed with excess deionized water and ethanol for several times and dried at 80 ℃ under vacuum for 8h.

Synthesis of -SO_3Li-functionalized mesoporous silicas (MCM41-SO_3Li, SBA15-SO_3Li)

1.0 g -SO_3H-functinalized mesoporous silicas (MCM41-SO_3H, SBA15-SO_3H) were placed in 20 mL prepared solution of 1 M LiCl in deionized water for ion exchange. The solution was refreshed three times. The solids were centrifugated, washed with deionized water and ethanol several times, and then dried at 80 ℃ under vacuum for 8 h.

Synthesis of -NH_2-functionalized mesoporous silicas (MCM41-NH_2)

1 g mesoporous silicas (MCM41) were added to a solution of APTES (2 mL) in dry toluene and refluxed for 24 h. The products were collected by centrifugation, washed with ethanol for several times and dried at 80 ℃ under vacuum for 8 h.

Synthesis of -NHTf -functionalized mesoporous silicas (MCM41-NHTf)

-NH_2-functionalized mesoporous silicas (0.65 g, about 1.0 mmol) (MCM41-NH_2), triethylamine (0.152 g, 1.0 mmol) and anhydrous dichloromethane (20 mL) were mixed and cooled down to 0 ℃. Then trifluoromethanesulfonic anhydride (0.339 g, 1.2 mmol) was slowly added to the mixture, followed by adding pyridine (0.079 g, 1.0 mmol) dropwise. The mixture was maintained at 0 ℃ for 30min and then reacted at room temperature for 72 h. After the reaction, the sample was collected by centrifugation and washed three times with dichloromethane and finally air dried[2].

Synthesis of -NLiTf-functionalized mesoporous silicas (MCM41-NLiTf)

-NHTf-functionalized mesoporous silicas (0.79 g, about 1.0 mmol) (MCM41-NHTf) were stirred in 0.06 M K_2CO_3 solution (20 mL) to neutralize protons for 12 h. The sample was obtained by centrifugation and washed with deionized water, followed by dried at 80 ℃ under vacuum for 8 h to get -NKTf-functionalized mesoporous silicas.

-NKTf-functionalized mesoporous silicas were placed into 1 M LiTFSI/CH_3CN solution to replace the K^+ with Li^+. The solution was refreshed three times. The samples were collected by centrifugation and washed three times with CH_3CN and finally dried at 80 ℃ under vacuum for 8 h.

Synthesis of MCM/PVDF/PPnw membrane

MCM41-NLiTf (400 mg), PVDF (100 mg) and LiTFSI (57 mg) were mixed in NMP (2.5 mL) to form a homogeneous gel. The gel was casted into cleaned glass covered with PP nonwoven. The casting gap of 300 μm was used for casting the membrane. Then the gel was dried at 80 ℃ under vacuum overnight. The obtained flexible membranes were stored in an argon filled glove box (< 0.1 ppm H_2O and O_2) (MIKROUNA).

Preparation of cathode

Commercial cathode material ($LiFePO_4$), super-P and PVDF were mixed in NMP with a mass ratio of 8:1:1 to obtain the cathode mixture. The cathode mixture was coated on an aluminum foil. The prepared electrode was dried at 80 ℃ under vacuum overnight. The electrode films were punched into disks with a diameter of 12 mm. The loading of the active material was around 2.4 mg cm^{-2}. The voltage window for the batteries equipped with LFP cathodes was set to 2.8 – 3.6 V.

Characterization

X-ray diffraction patterns were acquired by an X-ray diffractometer (EMPYREAN PANalytical) with Cu-Kα radiation (λ=1.54 Å). The morphologies of the samples were observed by field-emission scanning electron microscopy (SEM) (Phenom, PW-100-060). The surface composition and valence state were analyzed by X-ray photoelectron spectroscopy (XPS, Thermo Fischer ESCALAB 250 Xi) with Al Kα radiation. All XPS spectra were calibrated by shifting the detected adventitious carbon C 1s peak to 284.8 eV. Contents of metal ions in the samples were detected by inductively coupled

plasma atomic emission spectrometry (ICP-AES) on a Thermo Fisher ICAP RQ. Fourier Transform Infrared ((FT-IR) spectroscopy was tested on BRUKER TENSOR 27. Nitrogen adsorption–desorption measurements at 77 K were performed on a TriStar II 3020 surface area analyzer. Before analysis, samples were degassed at 120 ℃ for 24 h. Tensile tests of membranes were conducted on CMT6103 at room temperature with the rate of 0.2 mm min^{-1}.

Electrochemical measurements

Ionic conductivity and electrochemical window were tested with electrochemical workstation (BioLogic). The ionic conductivity was determined using electrochemical impedance spectroscopy (EIS) with pellets or membranes between two stainless steel (SS) electrodes in self designed models or 2032-type coin cell, respectively. The frequency range was from 20 kHz to 0.1 Hz and the AC amplitude was 10 mV. The ionic conductivity (σ, S cm^{-1}) was calculated by using the end point of the semicircle as the ion resistivity (R, Ohm), thickness (L, cm) and area (S, cm^2) of the pellets or membranes based on $\sigma = L/(R \times S)$.

Electrochemical window was measured by linear sweep voltammetry (LSV) using Li|electrolyte|SS cells with a scan rate of 1 mV s^{-1} range from open voltage to 5.5 V.

Lithium-ion transference number (t_{Li+}) was measured by combining an AC impedance measurement with the frequency range from 20 kHz to 0.1 Hz and a potentiostatic polarization measurement with a constant DC voltage of 50 mV using Li|electrolyte|Li cells. t_{Li+} was calculated based on the equation: $t_{Li+} = I_S (\Delta V - I_0 R_0)/ (I_0 (\Delta V - I_S R_S))$. ΔV was the DC polarization voltage (50 mV); I_0 and I_S were the initial and stable currents during polarization; R_0 and R_S were the interface impedances before and after polarization.

Density function theory (DFT) calculations

The DMol3 program was employed to perform the DFT calculations with meta-generalized approximation (m-GGA) density functional theory setup with the M06-L functional. The double numerical plus polarization (DNP) basis set was used to describe the atomic orbitals. The convergence criteria were the following: 1) an SCF tolerance of 10^{-6} au; 2) an energy change of 10^{-5} hartree; 3) a max force tolerance of 0.002 hartree/Å; and 4) a max displacement tolerance of 0.005 Å. The

molecules used for DFT calculations were simplified by connecting the anion groups ($-SO_3^-$, $-NTf^-$) with $-CH_2CH_2CH_3$ groups. The binding energy was calculated using: $E_B = E(Li^+\text{-anion}) - E(Li^+) - E(\text{anion})$.

Molecular dynamic (MD) simulations

MD simulations were performed based on the Large Scale Atomic/Molecular Massively Parallel Simulator (LAMMPS) code[3]. The model of anion functionalized MCM-41 was built by the following steps: 1) SiO_2 crystal with a size of 59.5 Å × 49.1 Å × 54.0 Å was first built; 2) pore structure was realized by deleting the atoms inside the cylinder with a radius of 1.25 nm; 3) 40 anion groups and Li^+ were generated inside the inner surface of the pore; 4) the remaining empty space was filled with 190 PC molecules, which approached with the bulk density of pure PC liquid.

The OPLS-AA force field[4, 5] was used to describe the energy potential of Li^+ and UFF force field[6] was used for the residual part. The bonded and non-bonded parameters for Li^+ and the remaining part were obtained from Jensen[7] et al. and Boyd[8] et al., respectively. The partial charges of Li^+ were set as +1 while that of the anion groups were fitted from DFT calculations result. The charges of silicas were set as 0 for convenience based on the fact that they only worked as porous backbone. A cutoff of 12 Å was used for both van der Waals interactions and long-range correction (particle-particle-particle-mesh) of Coulombic interactions.

The initial configurations were first minimized by conjugated-gradient energy minimization scheme employing a convergence criterion of 1.0×10^{-4}. The systems were then equilibrated in NPT ensemble using the Parrinello-Rahman barostat for 2 ns to maintain a temperature of 300 K and a pressure of 1 atm[9]. Another 5 ns production run in NPT ensemble at 298K was conducted finally. A time step of 1 fs was used for all simulations. An external electric field of 0.1 V $Å^{-1}$ was applied during the simulation. Using external electric field to calculate the mobility of ions was widely used in studying the ion transport in bulk aqueous solution and nano-channels[10]. Only the final 5 ns was sampled for mobility analyses. The mobility values (μ) were calculated based on: $\mu = V/E$, where E is the applied electric field strength and V is the drift velocity.

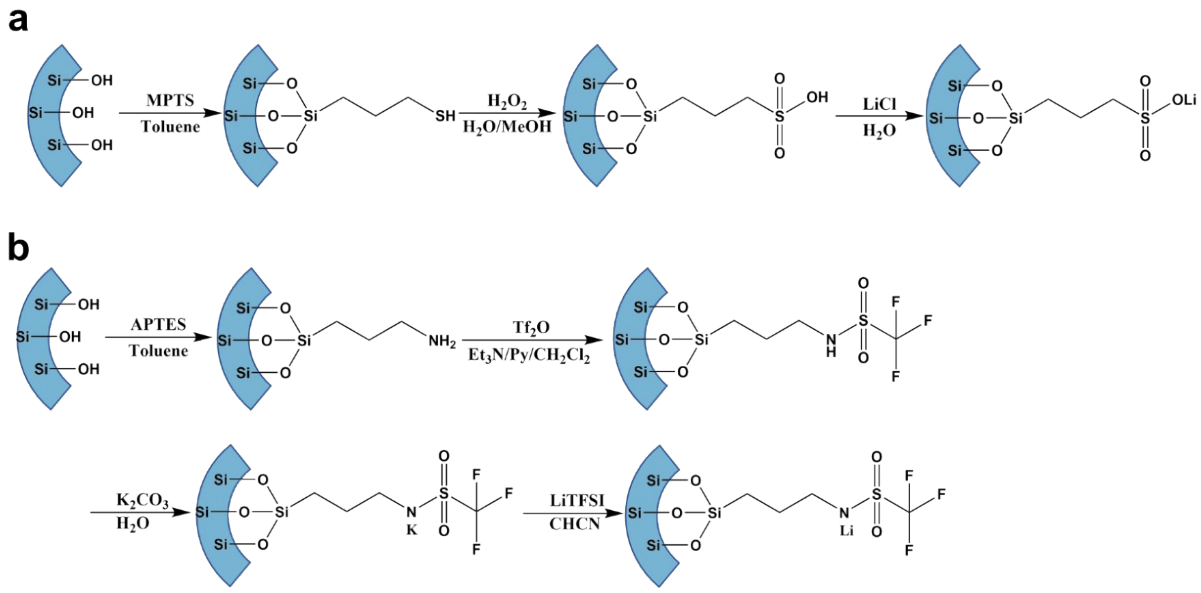

Figure S1. (a-b) Illustration of the synthesis procedure of the mesoporous silicas (MCM-41, SBA-15) based electrolyte functionalized with $–SO_3$- and –NTf$^-$ anion groups, respectively.

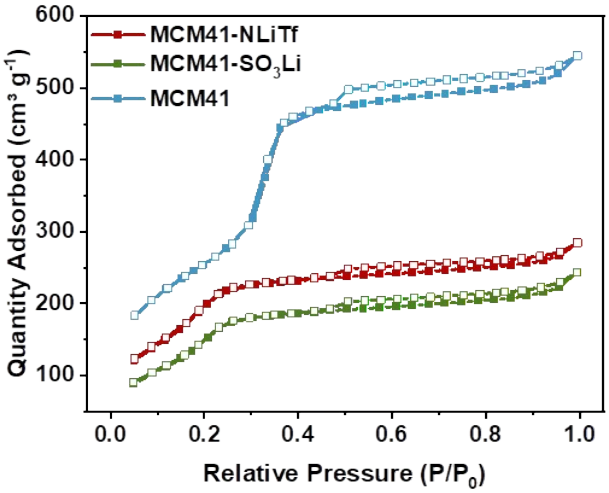

Figure S2. Nitrogen adsorption/desorption isotherms of MCM-41, MCM41-SO_3Li and MCM41-NLiTf.

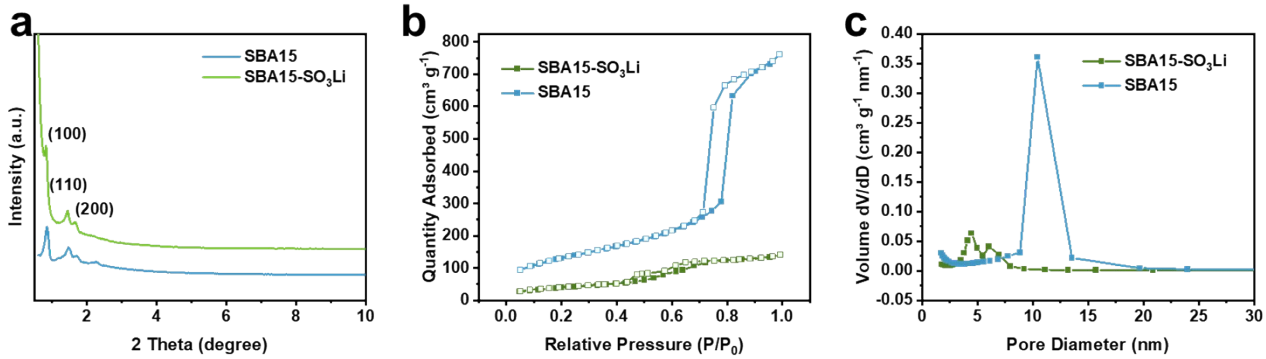

Figure S3. (a) XRD patterns of SBA-15 and SBA15-SO_3Li; (b) Nitrogen adsorption/desorption isotherms of SBA-15 and SBA15-SO_3Li; (c) Pore size distributions of SBA-15 and SBA15-SO_3Li.

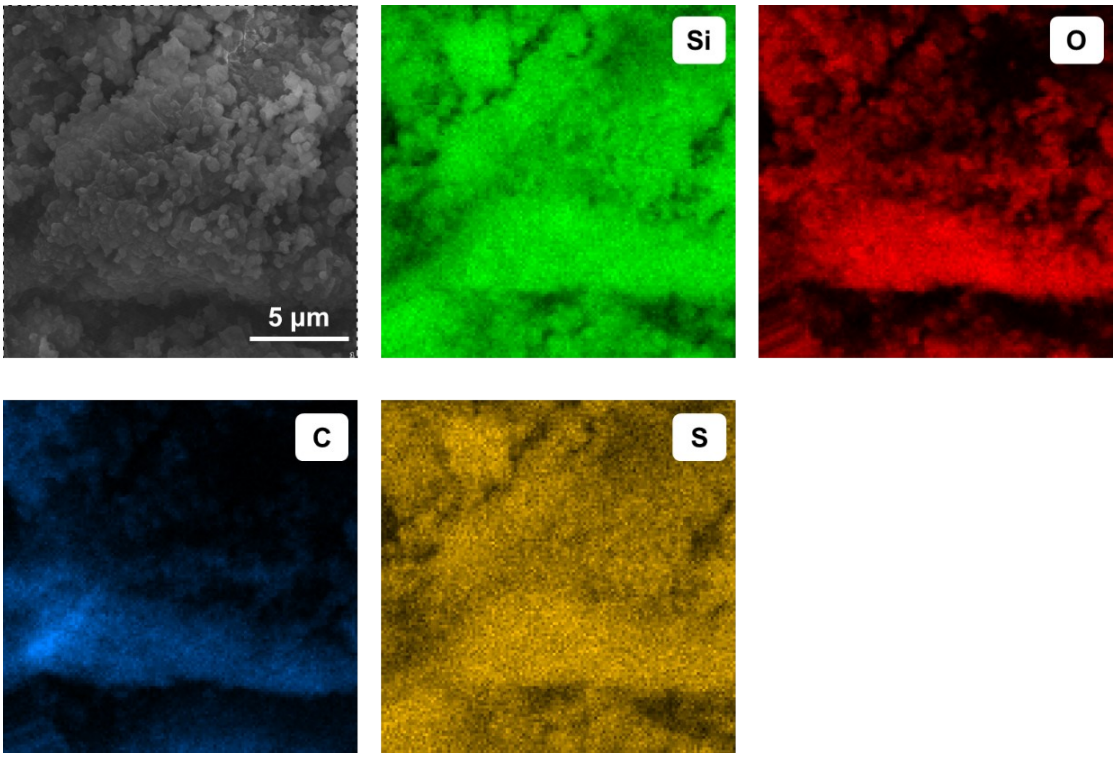

Figure S4. SEM images of MCM41-SH and corresponding elemental mapping analysis of MCM41-SH.

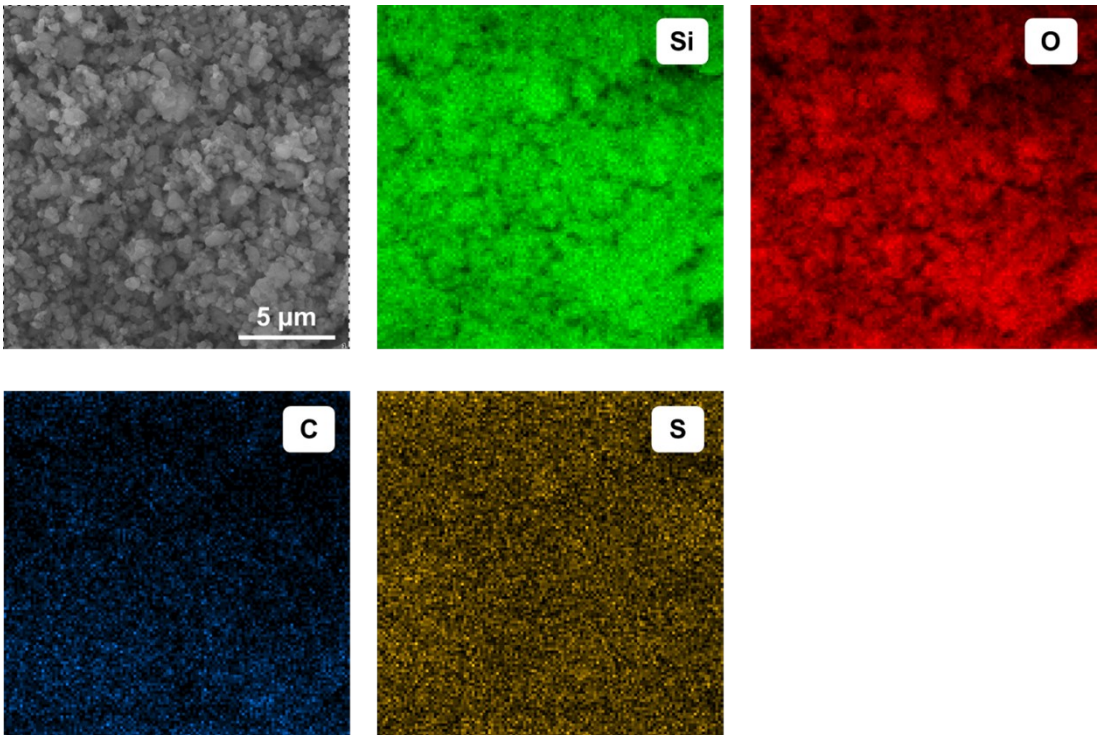

Figure S5. SEM images of MCM41-SO_3H and corresponding elemental mapping analysis of MCM41-SO_3H.

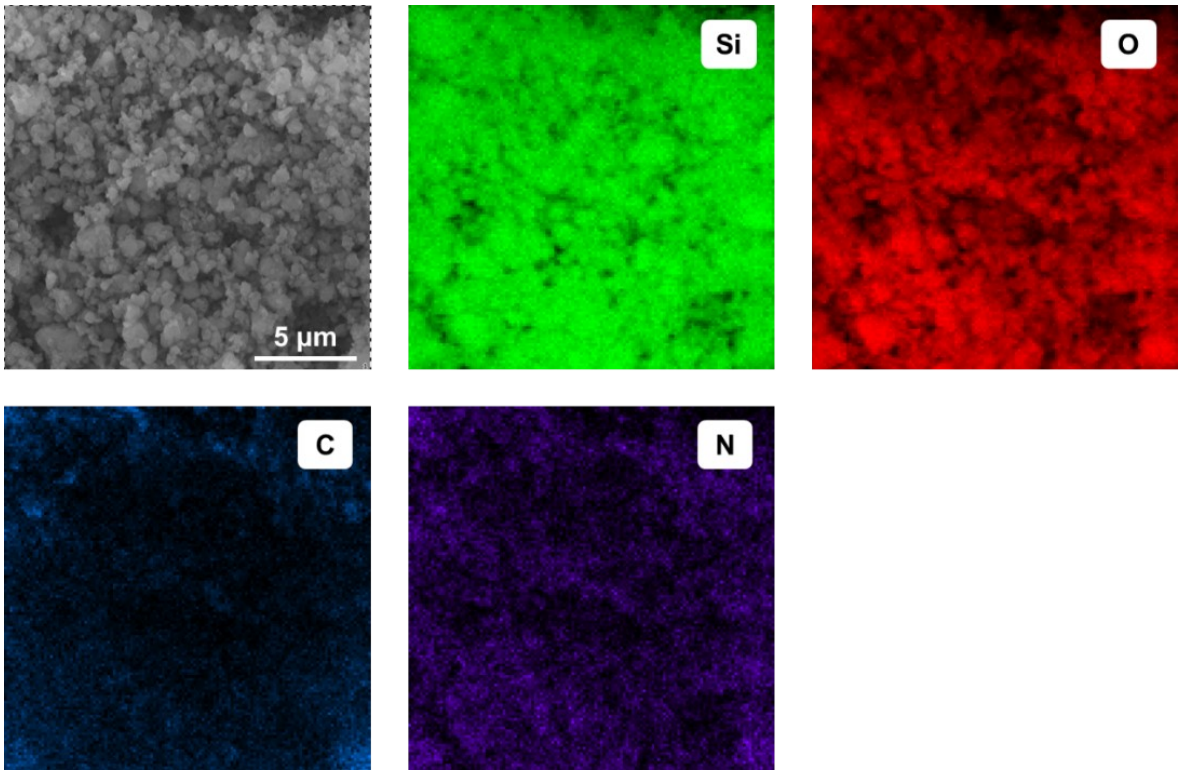

Figure S6. SEM images of MCM41-NH_2 and corresponding elemental mapping analysis of MCM41-NH_2.

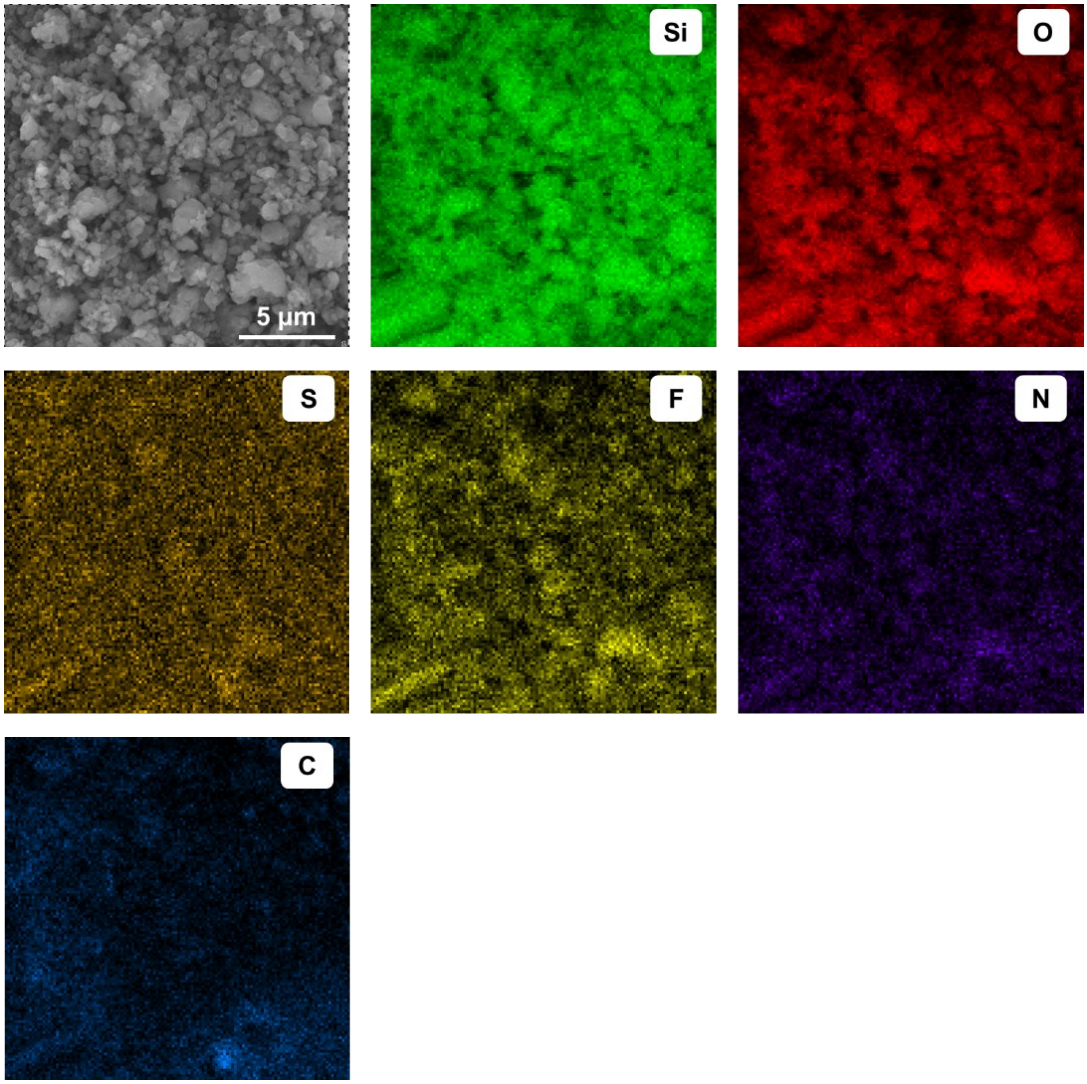

Figure S7. SEM images of MCM41-NHTf and corresponding elemental mapping analysis of MCM41-NHTf.

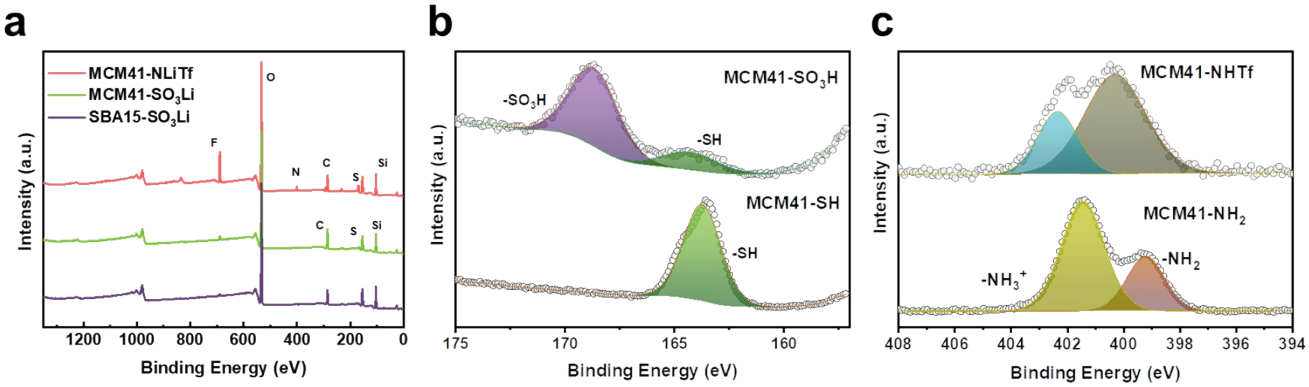

Figure S8. (a) XPS spectra of SBA15-SO_3Li, MCM41-SO_3Li and MCM41-NLiTf. (b) The S 2p XPS spectra of MCM41-SH and MCM41-SO_3Li.(c) the N 1s XPS spectra of MCM41-NH_2 and MCM41-NHTf.

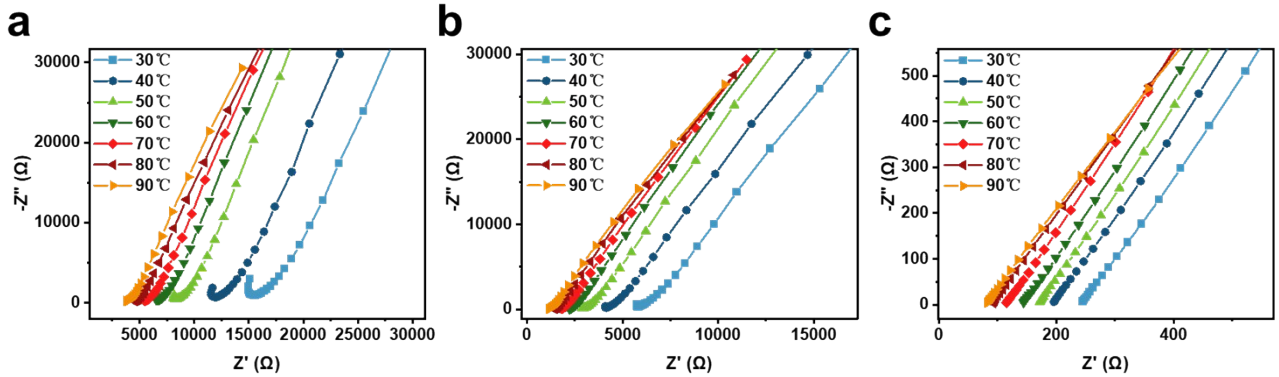

Figure S9. (a-c) EIS plots of SBA15-SO_3Li, MCM41-SO_3Li and MCM41-NLiTf under temperature range from 30 ℃ to 90 ℃, respectively.

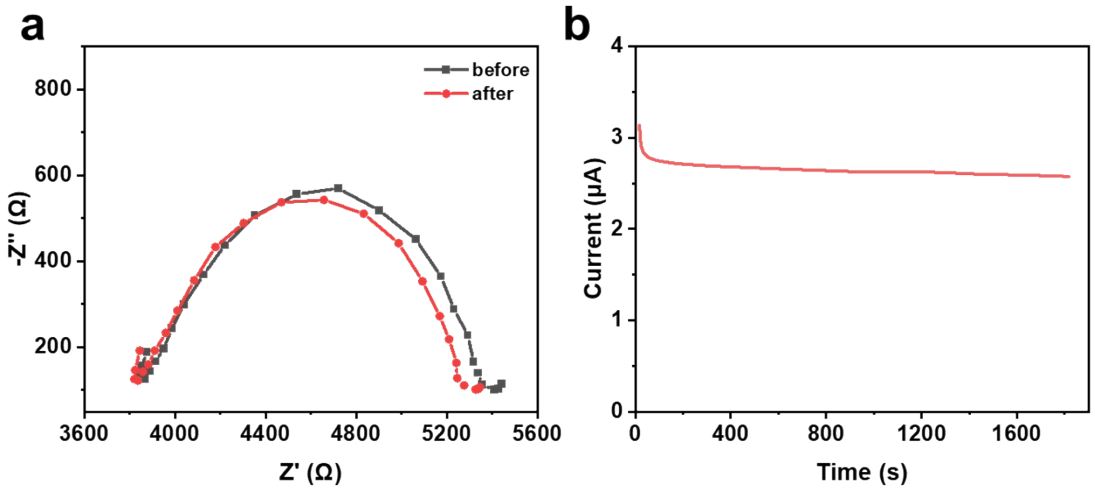

Figure S10. (a) Nyquist plots of the Li|MCM41-NLiTf|Li cell before and after polarization. (b) Polarization of the Li|MCM41-NLiTf|Li cell at an applied voltage of 50 mV. After a voltage of 50 mV was applied to the symmetric cell, the current response dropped from I_0=3.08 μA to its stead state I_s=2.57 μA, with interface resistance changing from R_0=1551 Ω to R_s=1481 Ω.

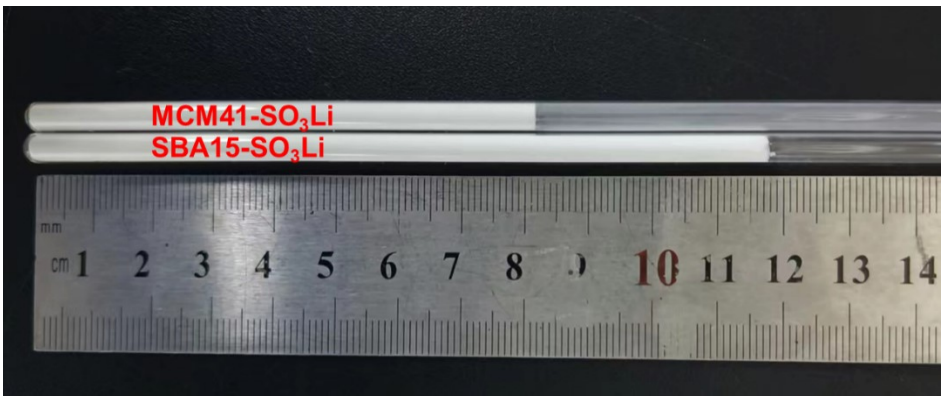

Figure S11. Comparison of MCM41-SO_3Li and SBA15-SO_3Li with the same weight (0.50 g).

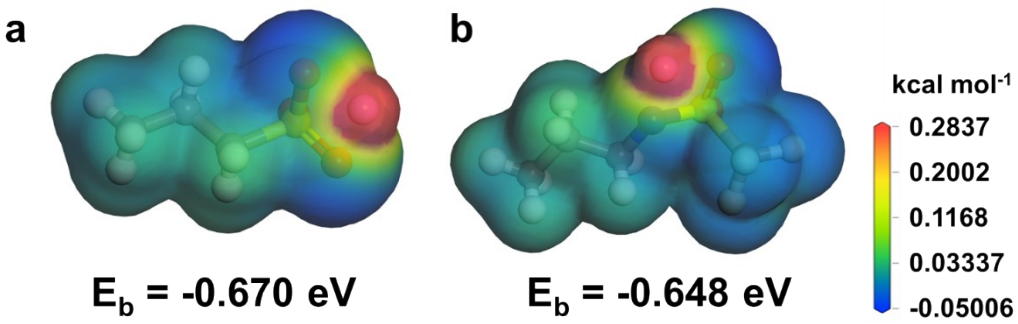

Figure S12. Electrostatic potential diagrams of –SO_3Li and –NLiTf and the corresponding binding energy.

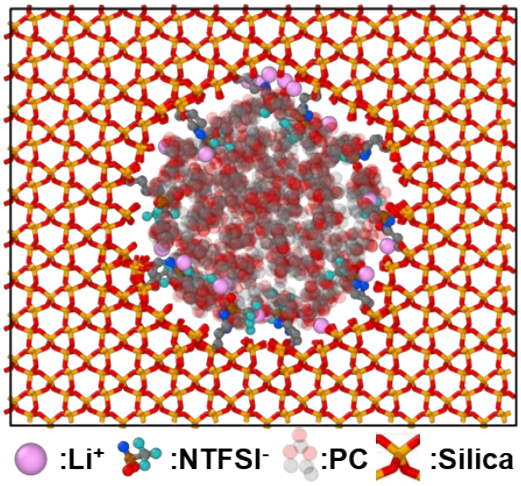

Figure S13. Illustration of the model used for molecular dynamics (MD) simulation.

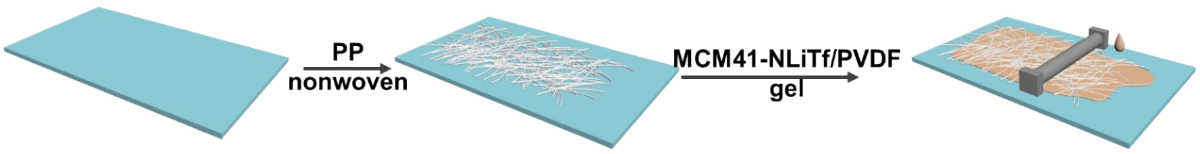

Figure 14. Schematic illustration of the preparation of MCM/PVDF/PPnw membrane.

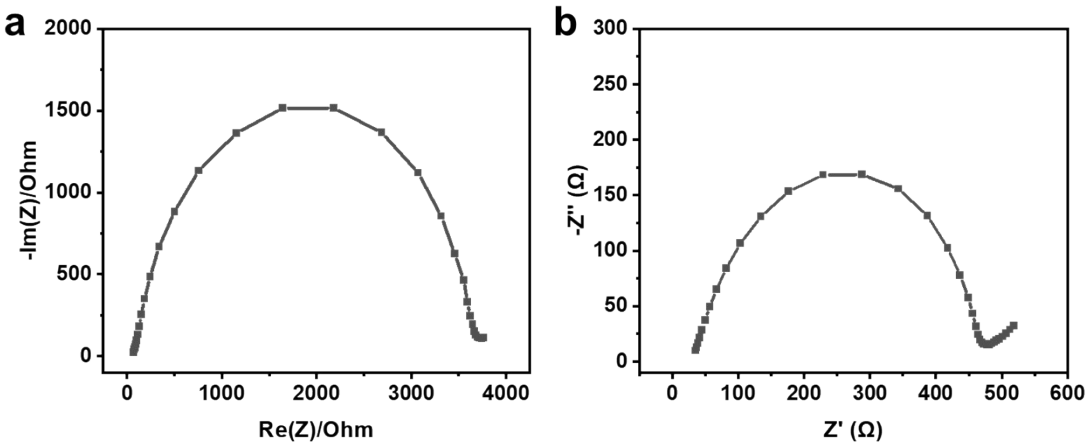

Figure S15. EIS plots of Li|MCM/PVDF/PPnw|Li symmetric cell (a) without and (b) with lithium salt. The addition of LiTFSI could ensure the ionic transport in PVDF binder.

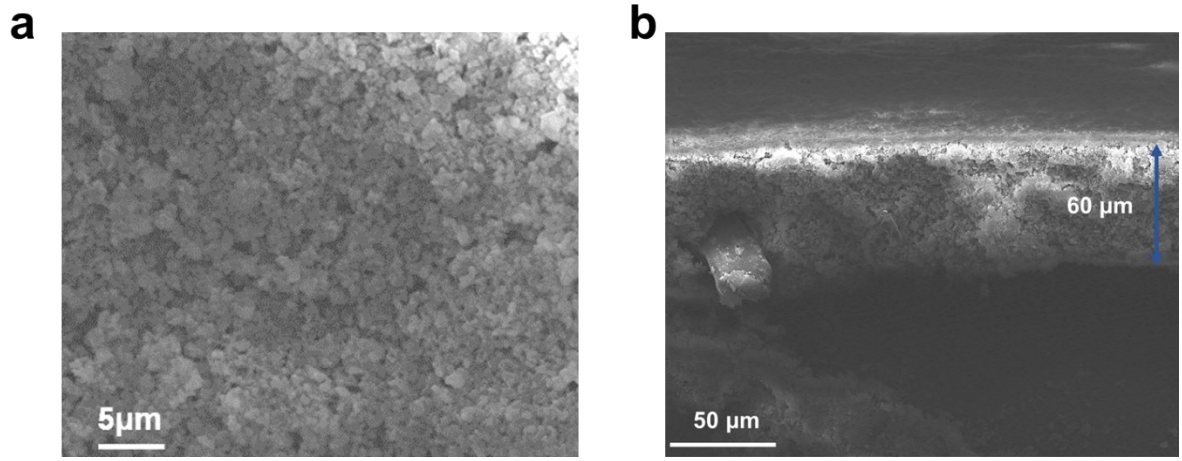

Figure S16. (a) Top view and (b) cross-section view of MCM/PVDF/PPnw membrane. MCM41-NLiTf particles were uniformly distributed in the as-fabricated MCM/PVDF/PPnw composite membrane and PPnw was embedded inside the membrane.

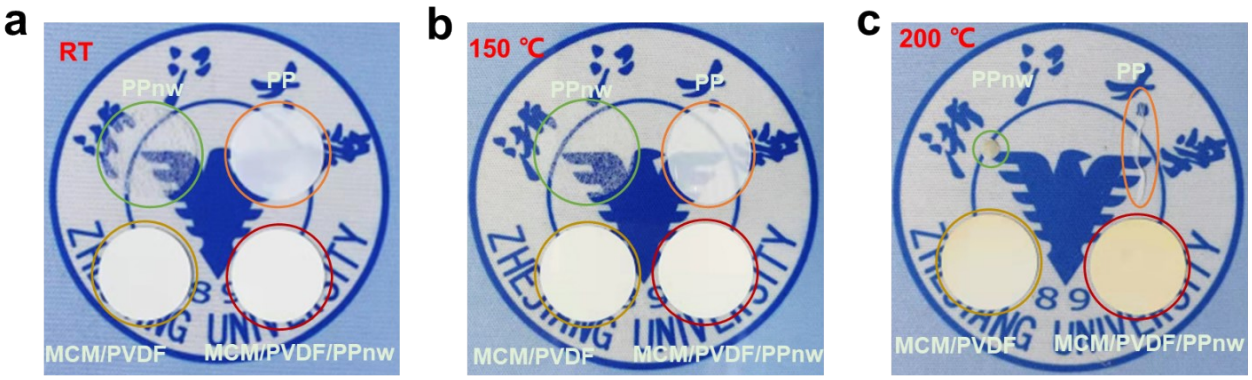

Figure S17. Thermostability of PP nonwoven, commercial PP, MCM/PVDF and MCM/PVDF/PPnw under (a) room temperature, (b) 150 ℃ and (c) 200 ℃.

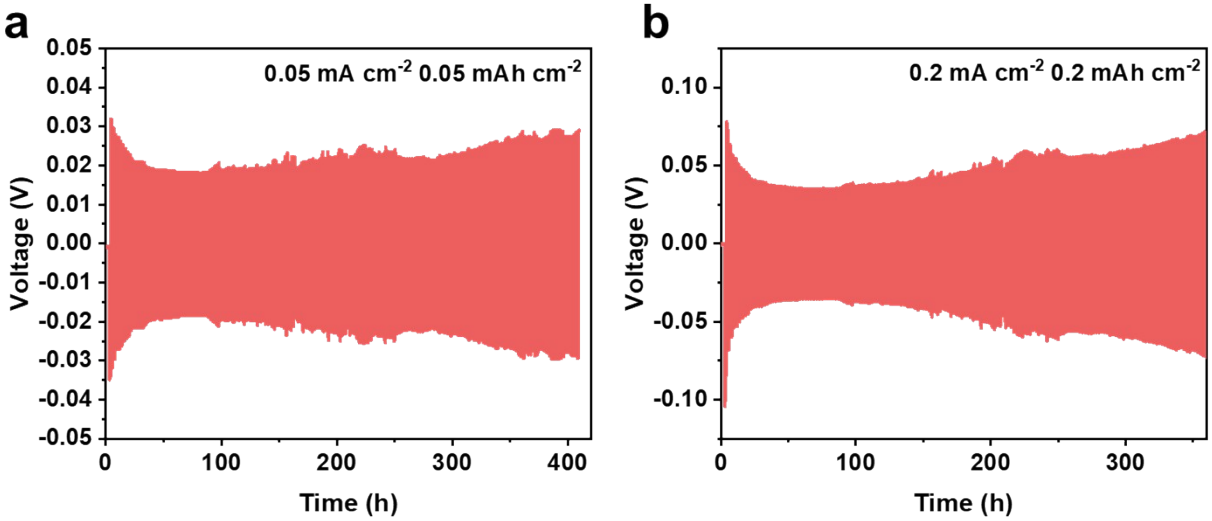

Figure S18. Galvanostatic cycling performance of the Li|MCM41/PVDF/PPnw|Li symmetric cell under current density of 0.05 mA cm^{-2}, 0.2 mA cm^{-2}, and current areal capacities of 0.05 mA h cm^{-2} , 0.05 mA h cm^{-2}, respectively.

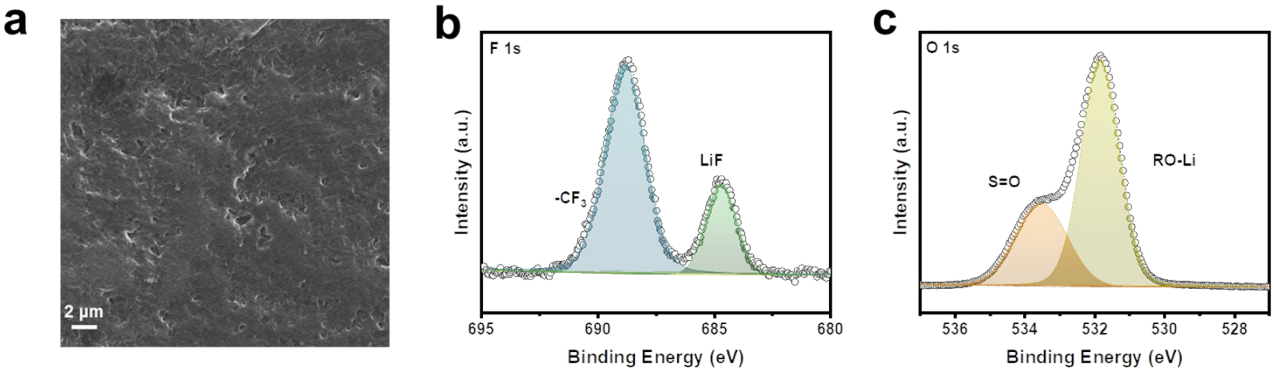

Figure S19. (a) SEM image and (b-c) XPS analysis of lithium anode after cycling under current density of 0.2 mA cm^{-2} and current areal capacities of 0.2 mA h cm^{-2} for 10 cycles.

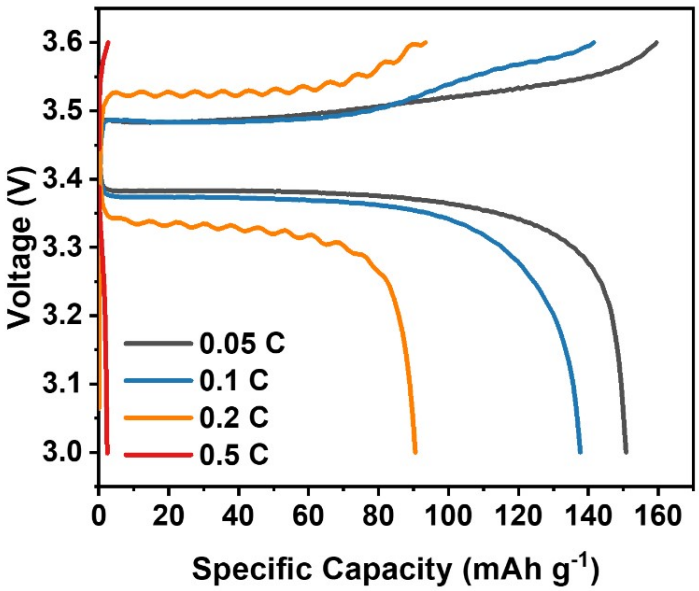

Figure S20. The corresponding charge-discharge voltage profiles for C rate performance.

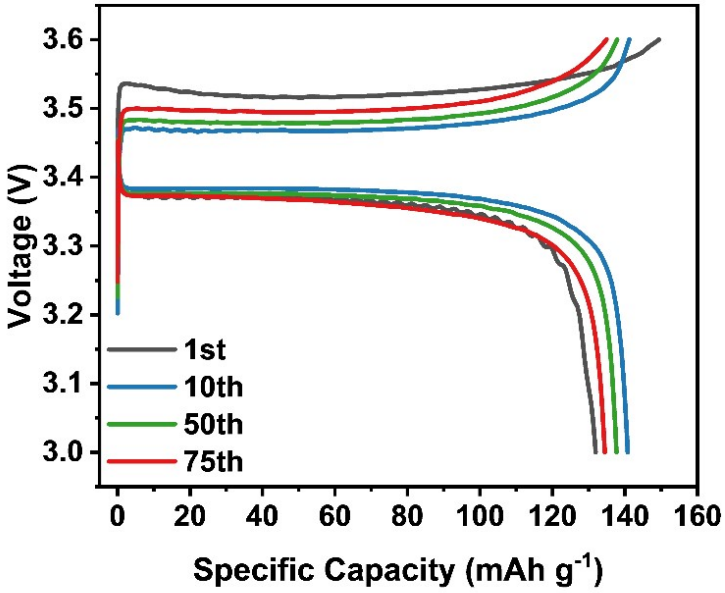

Figure S21. The corresponding charge-discharge voltage profiles for cycling performance under 0.1C.

References

1 1G. H. Mahdavinia and H. Sepehrian, *Chin. Chem. Lett.*, 2008, **19**, 1435-1439.

2 2F. Zhu, H. Bao, X. Wu, Y. Tao, C. Qin, Z. Su and Z. Kang, *ACS Appl. Mater. Interfaces*, 2019, **11**, 43206-43213.

3 3S. Plimpton, *J. Comput. Phys.*, 1995, **117**, 1-19.

4 4W. L. Jorgensen, D. S. Maxwell and J. Tirado-Rives, 1996, **118**, 11225-11236.

5 5G. A. Kaminski, R. A. Friesner, J. Tirado-Rives and W. L. Jorgensen, *J. Phys. Chem. B*, 2001, **105**, 6474-6487.

6 6A. K. Rappe, C. J. Casewit, K. S. Colwell, W. A. Goddard and W. M. Skiff, *J. Am. Chem. Soc.*, 1992, **114**, 10024-10035.

7 7K. P. Jensen and W. L. Jorgensen, *J. Chem. Theory Comput.*, 2006, **2**, 1499-1509.

8 8A. S. L. Gouveia, C. E. S. Bernardes, L. C. Tome, E. I. Lozinskaya, Y. S. Vygodskii, A. S. Shaplov, J. N. C. Lopes and I. M. Marrucho, *Phys. Chem. Chem. Phys.*, 2017, **19**, 29617-29624.

9 9J. L. Abascal and C. Vega, *J. Chem. Phys.*, 2005, **123**, 234505.

10 10X. Li, H. Zhang, P. Wang, J. Hou, J. Lu, C. D. Easton, X. Zhang, M. R. Hill, A. W. Thornton, J. Z. Liu, B. D. Freeman, A. J. Hill, L. Jiang and H. Wang, *Nat. Commun.*, 2019, **10**, 2490.